# Spectroscopy of heliumlike argon resonance and satellite lines for plasma temperature diagnostics

C. Biedermann and R. Radtke
*Max-Planck-Institut für Plasmaphysik, EURATOM Association, Bereich Plasmadiagnostik, Mohrenstraße 41, D-10117 Berlin, Germany*

K. B. Fournier
*Lawrence Livermore National Laboratory, Livermore, California 94550*

(Received 15 August 2002; published 11 December 2002)

The $n=2-1$ spectral emission pattern of heliumlike argon, together with the associated satellite emission originating from lithiumlike argon have been measured with high-resolution x-ray spectroscopy at the Berlin electron-beam ion trap. The observed line intensity across a wide range of excitation energies was weighted by an electron-energy distribution to analyze as a function of plasma temperature the line ratios between *KLL* dielectronic recombination satellites, in particular the $j+z$, $j$, and $k$ satellites, and the *w*-resonance line. A good agreement between various theoretical models is found, supporting the method of line-ratio measurement as a temperature diagnostic for plasmas. A value for the so-called *R*-line ratio is determined and calculations with the HULLAC suite of codes predict it to be electron density independent over a wide range.

DOI: 10.1103/PhysRevE.66.066404 PACS number(s): 52.70.La, 52.25.Os, 32.30.Rj, 34.80.Lx

## I. INTRODUCTION

The observation of characteristic x-ray emission lines from heliumlike charge states serves as a means to diagnose hot plasmas ranging from magnetically confined [1,2] or laser-produced plasmas, to plasmas of astrophysical objects, such as supernova remnants or solar flares [3–6]. Heliumlike ions with a well-studied level structure allow the calculation of atomic rates of recombination and ionization for a variety of plasma conditions, and the identification of a few distinct line-ratio combinations offers the possibility to determine the electron temperature or density of the plasma. The use of sensitive ratios for diagnostics is particularly important in x-ray astrophysical observations, where direct probes of plasma density and temperature are impossible [7]. Further, such spectra from tokamak-fusion devices can provide information on the transport and the spatial distribution of impurities, and can be used to detect possible deviations from the Maxwellian energy distribution of the exciting electrons by polarization spectroscopy [8,9]. However, theoretical predictions require knowledge of a multitude of accurate cross sections and need to be checked by benchmark experiments.

The spectrum of He-like ions is dominated by four lines labeled according to Gabriel [3]: the resonance line *w*, the intercombination lines *x* and *y*, and the forbidden line *z*. They originate from transitions between the $1s2\ell$ levels and the ground state $1s^2\ {}^1S_0$ and are plotted in the energy-level diagram of Fig. 1. These parent emission lines frame the lines of satellite transitions of the type $1s^22\ell$-$1s\,2\ell2\ell'$ that result from the radiative stabilization of doubly excited states in the Li-like ion. During the stabilization, the additional $2\ell$ electron (a nonparticipating, so-called spectator electron) perturbs the other orbitals by shielding the nuclear charge resulting in a transition wavelength somewhat longer than that of the parent transition. The doubly excited states $1s2\ell2\ell'$ are predominately formed via the resonant process of dielectronic recombination (*KLL* resonance), while the $1s2\ell$ levels in the He-like ions are mainly populated by electron-impact excitation. Observing the intensity ratio of an individual satellite line to the *w*-resonance line is sensitive to the energy of the exciting electron; the ratio is a decreasing function of the electron temperature. The measurement of unblended line ratios provides thereby information about the temperature of the plasma. Particularly suited for diagnostic purposes are the strong $j$ ($1s^22p\,^2P_{3/2}$-$1s2p^2\,^2D_{5/2}$) and $k$ ($1s^22p\,^2P_{1/2}$-$1s2p^2\,^2D_{3/2}$) satellites, which cannot be excited directly from the ground state of the Li-like ion through promotion of an innershell electron. However, for the argon system investigated here, the $j$ and $z$ lines are separated by only 0.2 mÅ and cannot be spectrally resolved in a Maxwellian plasma. This leaves the measurement of the $k$ satellite to the *w*-resonance line ratio as the most useful diagnostic.

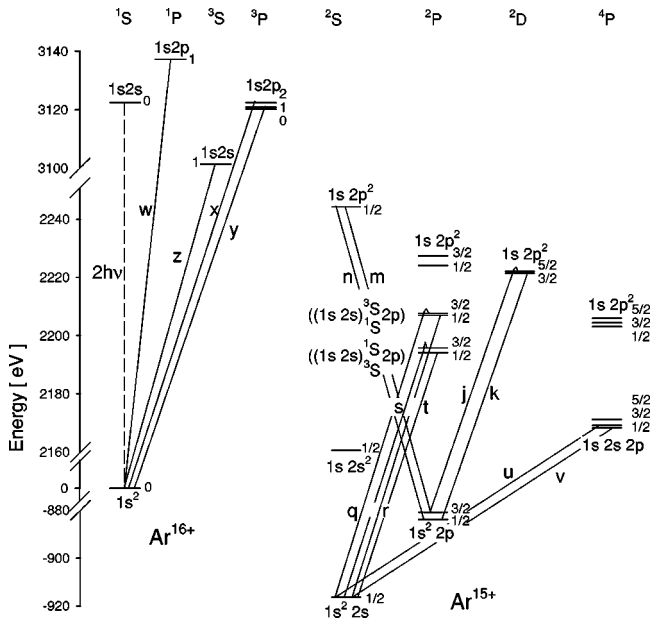


FIG. 1. Energy-level diagram of He-like $Ar^{16+}$ and Li-like $Ar^{15+}$ limited to transitions discussed in this paper. The level energy is plotted relative to the ground state $1s^2\,{}^1S_0$ of $Ar^{16+}$.

 

Argon is frequently employed in fusion devices, since it can easily be injected in controlled quantities, efficiently pumped out and serves as a tracer for plasma conditions diagnosing the ion temperature by Doppler broadening measurements [10] and plasma rotation profiles by looking at Doppler shifts of x-ray lines [11]. Further, argon is used as a coolant of the plasma edge in the divertor region for present-day tokamak machines [12]. The range of electron temperatures, where heliumlike argon is significantly abundant lies between 0.5 and 3.5 keV, covering a wide range of operating conditions such as central plasma temperatures in medium size tokamaks, e.g., the Torus Experiment for Technology Oriented Research (TEXTOR-94) [8], and temperatures obtained in outer regions of large machines such as the Joint European Torus (JET) [13]. While in such a plasma, the excitation is accomplished by a broad distribution of electron energies, usually a Maxwell-Boltzmann distribution, leading to the simultaneous emission of the directly excited resonance line and the dielectronic satellites, in the electron-bean ion trap, (EBIT) the ions are excited by a monoenergetic electron beam. By sweeping the electron-beam energy, it is possible to probe the trapped ion inventory, and, together with high-resolution x-ray spectroscopy, isolate certain electron-ion interactions. This allows the level-specific measurement of wavelength, excitation energy and strength of individual transitions. To evaluate line ratios for a plasma, the intensities from EBIT have to be folded with a function weighting the contribution according to the electron-energy distribution.

Dielectronic satellites and resonance lines of He-like argon have been studied in previous EBIT investigations focusing on the measurement of the $n=3-1$ lines [14] and more recently on the extraction of precise wavelengths to identify the spectral lines [15]. Here, we present results for the satellites *j* and *k* of He-like Ar, which are of considerable interest in tokamak research, expressed by the measurements at Alto Campo Torus (Alcator *C*, *C*-Mod) [1,11] and Tokamak Fontenay-aux-Roses (TFR) [10]. A recent study comparing the abundance of highly charged argon ions in JET tokamak and the Oxford EBIT [16] underlines the importance of x-ray emission spectra.

## II. EXPERIMENTAL CONDITIONS

The radiation pattern emitted by heliumlike argon was investigated by high-resolution x-ray spectroscopy using the Berlin electron-beam ion trap [17]. EBIT employs a magnetically compressed electron beam to produce, confine, and excite highly charged ions. The electron beam has a diameter of 70 $\mu$m and a density of $3\times10^{12}$ cm$^{-3}$ with a typical energy spread of 50 eV for the 90-mA current at 5-keV energy used in this experiment. Argon gas is continuously fed into the trap from a differentially pumped gas injector intersecting the electron beam. The charge state distribution is optimized for heliumlike argon by monitoring the x rays emitted during the radiative recombination process with beam electrons. Recording the evolution of the x-ray intensity for EBIT parameters such as trap depth, injected neutral argon density, and ionization energy, the time required to achieve maximum

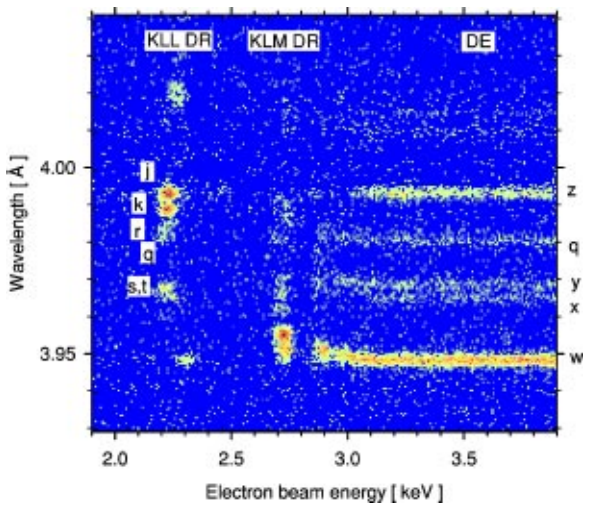


FIG. 2. Scatter plot of He-like and Li-like argon shown as wavelength of x-ray transitions as a function of the exciting electron-beam energy. Dielectronic satellite resonances appear as spots arranged in vertical groups according to the quantum number of the recombined electron. Directly excited transitions manifest as horizontal lines above threshold.

heliumlike argon abundance is found. For a 5-keV-energy, 90-mA-current electron beam and axial trapping potential of 200 V, the charge state distribution is dominated by $Ar^{16+}$ after 200 ms, with a pressure reading of $7\times10^{-6}$ Pa in the gas-injection pump step. This preparation of the trap inventory initializes each experiment sequence, which consists of a 20-ms period probing the argon ions and measuring the radiation followed by a 20-ms-reionization period. The sequence was repeated 80 times before the trap was dumped to prevent the accumulation of high-*Z* background ions and starting a new cycle ionizing to a fresh trap inventory.

The main experiment is conducted in two parts. In the first part, detailed information on the dielectronic resonance structures and the thresholds for direct excitation is obtained. After the preparation period, the monoenergetic electron beam is quickly ramped between 1.9- and 3.9-keV energy during the 20-ms probing period to examine the heliumlike argon ions and sample all the radiating processes of recombination and excitation with high-resolution spectroscopy. The slew rate of 100 eV/ms ensures that the investigated dielectronic resonances only alter the abundance of heliumlike argon by less than 1%. X rays are dispersed with a vacuum flat-crystal spectrometer reflecting the photons according to Bragg's law from a $75\times45$ mm$^2$ polished $10\bar{1}1$-quartz plate ($2d=6.6862$ Å), and the spectral information is recorded with a position-sensitive proportional counter. The spectrometer reaches a resolving power of $\lambda/\Delta\lambda\geqslant2000$, necessary to distinguish the *j* and *k* satellites of the *KLL* resonance. For every detected x ray, the position on the detector and the time during the ramp is recorded by an event-mode data acquisition system. This technique provides information on the wavelength of the x ray as a function of the exciting electron-beam energy. The data can be summarized with a scatter plot as shown in Fig. 2. The process of dielectronic recombination into the $n=2$ level

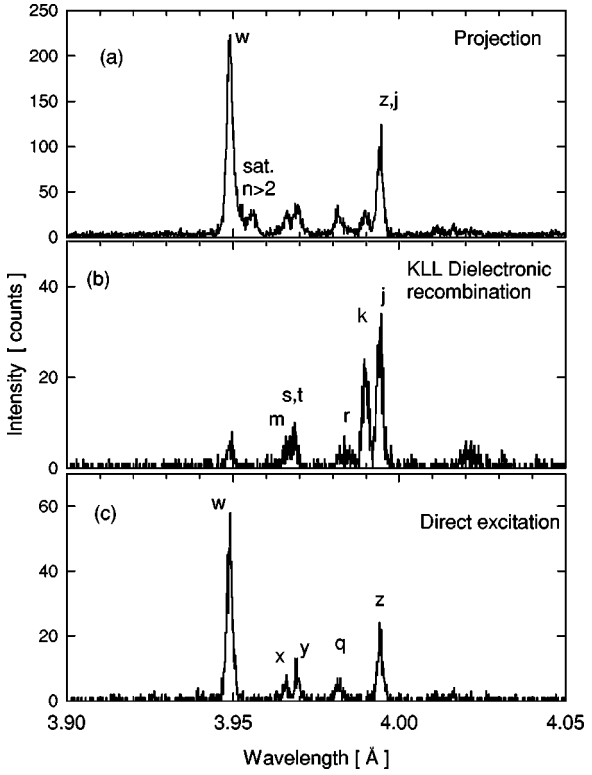


FIG. 3. Spectra of heliumlike argon. In (a) all the recorded x-ray intensity of Fig. 2 is projected onto the wavelength axis merging the lines of all different excitation processes into a one-dimensional spectrum. The spectrum of (b) shows only the lines arising from dielectronic recombination into the $n=2$ level $(KLL)$, whereas in (c) the lines emitted after direct excitation at 3.3-keV electron-beam energy are extracted. Lines are labeled according to Gabriel's notation [3].

$(KLL)$ of He-like argon producing the strong satellites *j*, *k*, *r*, *q* and *s*, *t* occurs at about 2.22-keV excitation energy (electron-beam energy). The satellites come into sight as vertical groups and can be well separated from the *KLM* and higher resonances, which converge to the threshold of direct excitation for the *w* line at 3.14 keV. Above threshold, *w*, *x*, *y*, and *z* as well as *q* manifest as horizontal lines. The latter appears through direct excitation of an innershell electron in the ground state of Li-like argon. In Fig. 2, only those transitions show up, where the $n=2$ electron stabilizes the doubly excited states $1s2\ell n\ell'$. Stabilization from higher *n* levels results in larger transition energies and, equivalently, smaller wavelengths ($n=3-1$ transitions show up at 3.4 Å). A weak trace of Be-like satellites appears at 4.02 Å and of Li-like $n=4-3$ satellites at 3.95 Å.

In a conventional one-dimensional spectrum, the various satellite intercombination and resonance lines cannot be well separated, as demonstrated in Fig. 3(a) by projecting all recorded x-ray events onto the wavelength axis. This information is similar to a typical spectrum obtained from a tokamak plasma (see e.g., Ref. [8], Fig. 2). The dielectronic recombination (DR) satellites with $n>2$ merge into a tail at the *w* line, and the *j* satellite cannot be separated from the forbidden line *z*. The various intensity contributions can only be disentangled by fitting peak functions to the spectrum. However, with EBIT it is possible to obtain wavelength dispersive spectra for distinct excitation energies as visualized in Figs. 3(b) and 3(c).

In the second part of the experiment, the electron beam is raised in eight steps of 2.56-ms duration from 3.8 to 15.8 keV to sample the radiation emitted after direct excitation over an extended range of excitation energies. Since the intensity of the *w*, *x*, *y*, *z*, and *q* lines decreases smoothly well above threshold as a function of the excitation energy, it is sufficient to probe the radiation at certain intervals and interpolate between them. Additionally, when rate coefficients for a plasma are calculated, the relative contribution of the line intensity at high excitation energies is reduced due to weighting with the energy-distribution function. Together with the information from the first part of the experiment, these data points provide excitation functions starting at the threshold energy and reaching up to 16 keV, from which line ratios can be extracted.

## III. DATA ANALYSIS

In a plasma, the rate coefficient for an electron-ion interaction process *i* is given as a probability or strength of excitation weighted by the energy distribution of the exciting electrons,

$$\alpha^i(T_e)=\langle v_e\sigma^i\rangle=\int_0^\infty v_e(E)\sigma^i(E)f_e(E,T_e)dE. \qquad (1)$$

The strength of excitation is expressed by the cross section $\sigma^i(E)$ at an electron energy $E$ corresponding to the velocity $v_e(E)$. This cross section is to be folded with the probability $f_e(E,T_e)$ of finding in a plasma of electron temperature $T_e$ an electron with energy $E$. $f_e(E,T_e)$ in a plasma follows a Maxwell-Boltzmann distribution.

On the other hand, in EBIT ions are excited by a monoenergetic electron beam of density $n_e(E)$ and the intensity $I^i(E)$ of a spectral line emitted as a result of an electron-ion interaction *i* can be expressed by

$$I^i(E)=v_e(E)n_e(E)\sigma^i(E)n_q. \qquad (2)$$

From this relation, we see that with EBIT, one can measure the rate of an excitation process $v_e(E)\sigma^i(E)$ by recording the intensity $I^i(E)$ normalized to $n_e(E)n_q$, where $n_q$ is the ion density:

$$v_e(E)\sigma^i(E)=\frac{I^i(E)}{n_e(E)n_q}. \qquad (3)$$

By quickly changing EBIT's electron-beam energy, the rates of processes can be measured as a function of excitation energy for a given population of ions. Folding the measured excitation function with $f_e(E,T_e)$ and integrating over $E$, we can calculate the rate coefficient for excitation at a temperature $T_e$:

$$\alpha^i(T_e)=\langle v_e\sigma^i\rangle=\int_0^\infty \frac{I^i(E)}{n_e(E)n_q}f_e(E,T_e)dE. \qquad (4)$$

We emphasize that the spectral information obtained with EBIT can be weighted with any given distribution function. Thereby, for instance, the effect of a non-Maxwellian electron-energy distribution on $\alpha^i$ can be studied. Sweeping EBIT's electron beam between 1.9 and 16 keV samples, all resonant and nonresonant radiation processes contributing to the excitation of heliumlike argon. Since in the present experiment, the electron-beam current $I_e$ is kept constant during the beam-energy ramp, the electron density varies as $n_e(E) \sim 1/\sqrt{E}$. This energy dependence can be combined with the Maxwellian distribution $f_e(E,T_e)$ to yield a weight function $G(E,T_e)=G_0\sqrt{E}f_e(E,T_e)$, with $G_0$ containing constant factors and the electron-beam current. The method of data sampling and analysis is similar to the one previously applied to obtain information on the radiation cooling rate of krypton [18].

Because the measurement of absolute line intensities is hampered by the problem of knowing the precise density of ions emitting the radiation and absolute detection efficiencies of the spectroscopic equipment, it is common to normalize the recorded intensity. Relating the satellite intensity to the *w*-resonance line appears natural, since the *w* line is brightest within the spectrum and is proportional to the number of heliumlike argon ions, from which the dielectronic satellites originate. For line ratios between a satellite *i* and the resonance line *w*, we obtain with Eq. (4) the expression

$$\frac{i}{w}=\frac{\alpha^i}{\alpha^w}\bigg|_{T_e}=\frac{I^i(E^i)G(E^i,T_e)}{\int_{E_{min}}^{E_{max}} I^w(E)G(E,T_e)dE}, \tag{5}$$

where the detected intensity of the satellite *i* with a resonance energy $E^i$ already integrates over the excitation energy, since the width of EBIT's electron-beam energy ($\sim$50 eV full width at half maximum) is much wider than the intrinsic width of the dielectronic resonance line. The integration limits for the *w* line are given by the threshold energy for direct excitation ($E_{min}$) and the maximum energy of the ramp ($E_{max}$). For this investigation, $E_{max}$ was limited to 16 keV because the weight function for plasma temperatures, where heliumlike argon is abundant suppresses intensity contributions at higher energies to negligible contributions. Cutting off the integration of the weighted line intensity at 16-keV excitation energy for a 3-keV-plasma temperature reduces the $\alpha^w$ contribution by only 0.6%.

The line radiation resulting from the excitation of an ion population with an electron beam is observed with a spectrometer and recorded on a detector. These experimental peculiarities modify the perceived intensity and can be expressed by an instrumental response function $D^i$ including the solid angle, collection efficiency, and diffraction properties as well as emission characteristics of the radiationlike effects of polarization. The observed intensity of a line $I^i_{obs}=D^iI^i$ is reduced due to the spectrometer response. At 90° to the electron beam, the intensity $I(90°)=I_{||}+I_\perp$ can be split into components polarized parallel and perpendicular to the electron-beam direction used as reference axis. After diffraction by a crystal for analysis, the observed intensity is

$$I_{obs}=\Omega\,\eta(I_{||}R_{||}+I_\perp R_\perp), \tag{6}$$

where $R_{||}, R_\perp$ are the integrated reflectivities of the respective polarization directions, $\Omega$ includes the geometry with the solid angle of acceptance of the spectrometer, and $\eta$ is the detection efficiency accounting for the transmission of foils and absorption in the detector gas. Further, it has to be taken into account that the line radiation originating from electric dipole transitions, such as the lines investigated here, are excited by a directed electron beam. In this case the total line intensity $I$ averaged over $4\pi$ relates with the intensity observed at 90° via $I/4\pi=I(90°)(3-P)/3$ [19]. The degree of polarization $P$ is defined as $P=(I_{||}-I_\perp)/(I_{||}+I_\perp)$ with a specific value for each transition and varying with energy of the exciting electron. The instrumental response function $D^i$ linking the observed intensity $I^i_{obs}$ to the total intensity $I^i$ of a line *i* is then given by

$$D^i=\frac{3\Omega\,\eta}{2(3-P)}R_{||}\left[1+P+(1-P)\frac{R_\perp}{R_{||}}\right]. \tag{7}$$

The geometrical factor $\Omega$ is the same for all investigated lines and cancels out when determining line ratios. The efficiency $\eta$ varies slightly, by 1.9%, between detecting the x-ray energies of the *w* line and the *j* satellite according to photo-absorption cross sections of Ref. [20]. Similarly, the integrated reflectivity $R_{||}$ is constant within less than 1% for the investigated wavelength range, while the reflectivity ratio $R_\perp/R_{||}$ increases by 10%. Values for the reflectivities of the quartz crystal are taken from theoretical calculations made available at Ref. [21]. The polarizations for the satellite lines are tabulated by Inal and Dubau [22]. The polarization degree of the resonance line excited by a monoenergetic electron beam is predicted to vary with the energy from 0.53 at excitation threshold (3.14 keV) to 0.58 at 4.2 keV energy falling off to a value of 0.25 at 16 keV using scaled values for heliumlike iron [22,23]. A minor reduction of the polarization of electric dipole transitions due to a deviation from the unidirectional electron collisions caused by the thermally induced transverse electron velocity component is not accounted for in the analysis, since the contribution is shown to be small for typical EBIT operating conditions [24].

The measured intensity of a line $I_{obs}$ is extracted from two-dimensional scatter-plot data like the one presented in Fig. 2 by projecting the number of observed photons within a narrow wavelength range specific for the particular transition onto the electron-beam energy axis. Thereby, the intensity in a region is summed along the wavelength axis resulting in one-dimensional spectra representing the excitation function. Satellite lines manifest as peaked distributions fitted to a voigt profile to determine the observed satellite intensity. For lines extending over a large beam-energy range, such as the *w*-resonance line, additional data to the one presented in Fig. 2 has been obtained at distinct electron-beam energies and provides supporting points to fit excitation functions over a wide range of energies. These measured number of photons are corrected for the spectrometer response, weighted according to the plasma temperature and integrated from threshold to $E_{max}$ to determine the rate of the process.

TABLE I. Line ratio $R=z/(x+y)$ for heliumlike argon. Comparison of values from EBIT facilities and a tokamak experiment with theoretical predictions. In the EBIT experiment, the electron-beam energy is $E_e=7$ keV and the current $I_e$. $T_e$ marks the electron temperature of the Maxwellian-distributed plasma.

| Data source | $R=z/(x+y)$ | $n_e$ ($\mathrm{cm}^{-3}$) | Remark |
|---|---|---|---|
| NIST-EBIT | $1.09\pm0.3$ | $2\times10^{12}$ | $I_e=59.8$ mA |
| Berlin EBIT | $1.38\pm0.25$ | $3\times10^{12}$ | $I_e=90$ mA |
| Alcator *C* | 1.21 | $1.5\times10^{14}$ | $T_e=1.4$ keV |
| Pradhan | 1.3 | $10^{11}-10^{15}$ | $T_e=1.4$ keV |
| HULLAC basic | 1.03 | $3\times10^{12}$ | $T_e=2$ keV |
| HULLAC $2h\nu$ | 1.37 | $3\times10^{12}$ | $T_e=2$ keV |
| HULLAC col | 1.35 | $3\times10^{12}$ | $T_e=2$ keV |
| HULLAC $2h\nu$ | 1.37 | $1\times10^{10}$ | $T_e=2$ keV |
| HULLAC $2h\nu$ | 1.30 | $1.5\times10^{14}$ | $T_e=1.5$ keV |

## IV. LINE RATIOS

### A. Density-dependent ratios

One of the most commonly used line ratios in astrophysics is to derive information from the $n=2-1$ x-ray emission of heliumlike ions is the ratio of the forbidden line *z* and the intercombination lines *x* and *y*, called $R=z/(x+y)$, which is predicted to be sensitive to the electron density [25]. However, this sensitivity, which is caused by collisional transfer from the metastable $1s2s\,^3S_1$ level to $1s2p\,^3P_J$ levels, is only efficient for light elements ($Z<12$) at densities relevant for fusion experiments ($n_e\sim10^{13}$ $\mathrm{cm}^{-3}$). For heliumlike argon, we extract from our EBIT measurements a value of $R=1.38\pm0.25$ for an electron density of $3\cdot10^{12}$ $\mathrm{cm}^{-3}$ calculated from the electron-beam current and the estimated beam radius. This value agrees with the theoretical ratio $R=1.3$ using excitation rates by Pradhan [1], which for argon is independent of density up to $n_e=10^{15}$ $\mathrm{cm}^{-3}$. In Table I, we compare the *R* value and find consent with a measurement at the NIST-EBIT [7] using a microcalorimeter with lower resolving power of the argon lines and a value from the Alcator *C* tokamak [1]. Further, predictions by the HULLAC package (detailed in the following sections) are listed and demonstrate the importance to include the two-photon decay of the $1s2s\,^1S_0$ level to the ground state (HULLAC $2h\nu$). The calculation including collisional data of Keenan *et al.* [26] (HULLAC col) has only a minor influence. Predictions at $n_e=10^{10}$ $\mathrm{cm}^{-3}$ and $10^{15}$ $\mathrm{cm}^{-3}$ differ only marginally and underline the insensitivity of *R* in the case of argon.

### B. Temperature-dependent-ratio theory

In what follows, we compare calculated ratios of intensities of Li-like dielectronic satellite lines to the He-like *w*-resonance line as a function of plasma electron temperature. Application of our argon models has been previously reported for the case of dielectronic and innershell-excited satellites to the $Ar^{16+}$ $n=3-1$ line in a high-density laser-produced plasma [27]. We compare ratios calculated in both the zero-density or coronal limit, and full collisional-radiative (CR) ratios to our measured data. For the low densities obtained in EBITs, we find that the predictions of the two cases differ by less than 10%. *Ab initio* atomic structure data for the lithiumlike, heliumlike, and hydrogenlike isoelectronic sequences of Ar have been generated using the HULLAC [28–32] suite of codes. All singly and doubly excited energy levels with principal quantum number $n\leqslant6$ have been treated.

The ionic transition rates above, including the autoionization rates from the Li- to He-like and He-like to H-like ions, as well as direct, impact ionization, and radiative recombination rate coefficients, are used to construct the CR rate matrix,

$$\frac{dn_j}{dt}=\sum_i n_iX_{i\to j}-n_j\sum_i X_{j\to i}, \tag{8}$$

where $n_j$ is the population in level *j*, and $X_{i\to j}$ is the total rate for transitions between levels *i* and *j*. The inverse of each ionization process, namely, dielectronic attachment and three-body recombination, have been found by enforcing detailed balance. Radiative recombination from and collisional ionization to the bare nucleus $Ar^{18+}$ is also included in the rate matrix. The relative populations of the four charge states and the population in each level of each ion are then found in the steady state. The resulting collisional-radiative line emission $\varepsilon_{ij}$ for each He- and Li-like transition is found at the specific transition wavelength, $\lambda_0$, for a given temperature and density,

$$\varepsilon_{ij}(\lambda_0)=n_iA_{ij}, \tag{9}$$

where $n_i$ is the (relative) population in the upper level and $A_{ij}$ is the radiative transition rate from level *i* to level *j*. Our steady-state CR intensities are then used to calculate the ratios of the Li-like $Ar^{15+}$ satellites to the $Ar^{16+}$ resonance line *w*.

In the low-density limit, i.e., the coronal approximation, the lithiumlike satellites to the heliumlike resonance lines investigated here can be created by two mechanisms, innershell electron-impact excitation followed by radiative stabilization or dielectronic recombination from the heliumlike ion. At EBIT's density, the *j* and *k* satellites discussed below can only be excited through dielectronic recombination. The emissivity of a line from level *j* of ion *q* excited by electron-impact excitation is given by

$$\varepsilon_{\mathrm{IE}} = n_e n_q C(T_e) \beta_{j,f}, \tag{10}$$

where $n_e$ and $n_q$ are the electron and ion densities, $C(T_e)$ is the impact excitation rate coefficient, and $\beta_{j,f}$ is the radiative branching ratio from the upper level of the observed transition,

$$\beta_{j,f} = \frac{A_{j,f}^{rad}}{\sum_i A_{j,i}^{auto} + \sum_f A_{j,f}^{rad}}. \tag{11}$$

The sum over $i$ in Eq. (11) runs over all levels in the next higher ion reachable from level $j$ by autoionization, and the sum over $f$ runs over all bound levels reachable from $j$ by radiative decay.

The emissivity $\varepsilon_{\mathrm{DR}}$ of a lithiumlike satellite excited by dielectronic recombination can be expressed as

$$\varepsilon_{\mathrm{DR}} = n_e n_{16+} F_1(T_e) F_2(j,f), \tag{12}$$

where all the temperature dependence is contained in

$$F_1(T_e) = \frac{1}{2}\left(\frac{4\pi a_0^2 \mathcal{R}}{T_e}\right)^{3/2} \exp(-\Delta E_{i,j}/T_e), \tag{13}$$

where $a_0$ is the Bohr radius, $\mathcal{R}$ is the Rydberg energy constant, and $\Delta E_{i,j}$ is the capture energy of the free electron, i.e., the energy difference between the $1s^2$ level and a $1snl'l'$ level. The satellite-intensity factor due to dielectronic recombination from level $i$ of ion $(q+1)$ via level $j$ of ion $q$ to level $f$ is given by

$$F_2(j,f) = \frac{g_j}{g_i} A_{j,i}^{auto} \beta_{j,f}, \tag{14}$$

where the $g$'s are the statistical weights of the intermediate (autoionizing) and initial (recombining) levels, and $A_{j,i}^{auto}$ is the rate of autoionization from level $j$ to level $i$.

In the limit, where all the excitation arises from the He $1s^2$ state, a lithiumlike dielectronic satellite line $(j \rightarrow f)$ and the corresponding heliumlike resonance line $(w)$ can be used as a convenient temperature diagnostic of the local plasma conditions by dividing Eq. (12) by Eq. (10),

$$\frac{\varepsilon_{\mathrm{DR}}^{jf}}{\varepsilon_{\mathrm{IE}}^{w}} = \frac{F_1(T_e) F_2(j,f)}{C_w(T_e)}, \tag{15}$$

where the branching ratio for the heliumlike resonance line is assumed to be 1. This ratio is independent of the ionization balance between the He- and Li-like ions, and is also independent of the electron density. For the densities of EBIT and tokamak plasmas, Eq. (15) is a good approximation of the satellite to resonance line intensity ratio. We compare the diagnostic ratio computed by Eq. (15) using the autoionization data generated *ab initio* with RELAC [30,31] to the same ratio computed with the autoionization rates of Chen [33]. For both the $k$ and $j$ satellite lines, the RELAC autoionization rates are $\sim 4\%$ larger than those of Chen, a difference much less than the error bars on the present measurements.

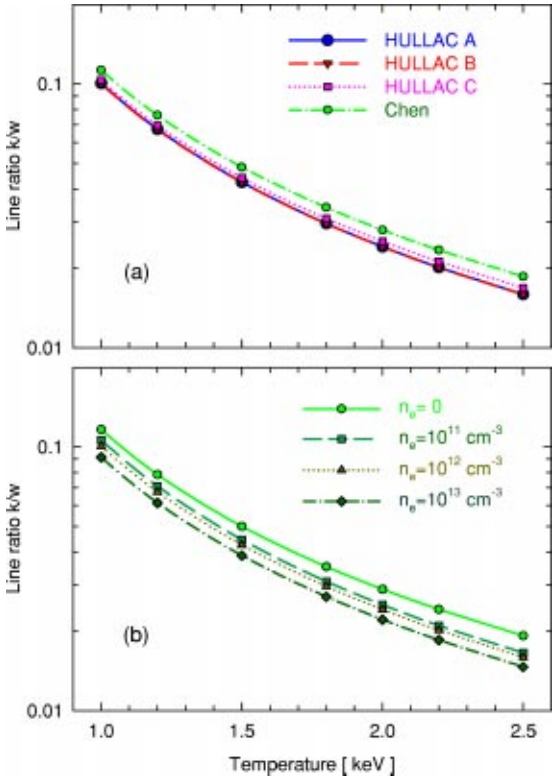


FIG. 4. (a) Comparison of the $k/w$ line ratio calculated with different theoretical models as function of the plasma temperature for an electron density of $n_e = 10^{12}$ cm$^{-3}$. The data using only HULLAC-calculated collisional excitation rates [32] (HULLAC *A*) and the calculation employing slightly different atomic potentials and radiative cascade models (HULLAC *B*) fall right on top of each other. In a third calculation, the collision data of Keenan *et al.* [26] (HULLAC *C*) are substituted for a few transitions in the HULLAC model. Also shown is the zero-density-limit ratio found using Chen's DR data [33] (Chen). (b) Comparison of the basic HULLAC CR model results for three densities, showing how collisional processes and cascades have only a small effect on the $k/w$ ratio. Also shown is the zero-density-limit ratio $(n_e = 0)$.

Figure 4(a) compares three collisional-radiative calculations of the $k/w$ ratio, and it is clear that the prediction of the $k/w$ ratio is insensitive to the assumptions made in the CR model. Two of the curves in Fig. 4(a) overlay each other, these curves were computed with the HULLAC model as described above, and with atomic potentials and additional high-$n$ cascade channels as described in Ref. [34]. The electron-impact excitation data in the basic HULLAC model for the He-like $Ar^{16+}$ ions has also been modified with the *R*-matrix calculations of Ref. [26]. From the trace labeled "HULLAC *C*" in Fig. 4(a), it is obvious that the collisional excitation rates as given by HULLAC are very close to Keenan *et al.*'s data. Finally, the uppermost trace in Fig. 4(a) shows the zero-density-limit $k/w$ ratio computed using Chen's data [33] in Eq. (15). The difference between the basic HULLAC CR value for EBIT and the value of the ratio given by Eq. (15) ranges from $\leqslant 10\%$ to $\sim 15\%$ as the temperature increases. Figure 4(b) shows the effect on the CR calculations of increasing density. The four traces in the figure are, from top to bottom, the zero-density-limit (labeled $n_e = 0$) ratio

with HULLAC autoionization data and the basic HULLAC CR calculations at $10^{11}$, $10^{12}$, and $10^{13}$ cm$^{-3}$. The CR ratio at $10^{12}$ cm$^{-3}$ differs from the low-density limit by $\approx$ 10%, and a change of two orders of magnitude in density in the CR calculation results in a decrease of nearly 15% in the predicted ratios. The $\approx$10% range of uncertainty in our theoretical treatments of the $j/w$ and $k/w$ ratios is less than the error bars on the measurements below.

### C. Temperature-dependent-ratio results

In the following, we concentrate on line ratios that involve dielectronic satellites. An obvious choice is the ratio of the sum of the satellite $j$ and the forbidden line $z$ normalized to the resonance line $w$. These lines are resolved with modest detection effort and their resonance strength leads to large intensities. Since the $j$ and the $z$ lines blend for the argon system and cannot be separated with common spectroscopic techniques, they are usually treated together. We have extracted the line ratio of $(j+z)/w$ from our measurement by summing the $j$ satellite and the integrated $z$ intensity. The result is plotted as a function of the plasma temperature in Fig. 5(a). For a plasma temperature of $T_e = 1.25$ keV TFR [10] reports a ratio $(j+z)/w = 0.56$, which is close to a theoretical value of 0.5 calculated by Bely-Dubau *et al.* [35] and agrees with the experimental value of the Berlin EBIT. The line ratio $(j+z)/w$ shows only a weak temperature dependence above about 1 keV, since the contribution of the $j$ satellite becomes less important for higher $T_e$ as compared to the nearly constant relative intensities of the $z$ and $w$ lines.

Apart from the statistical uncertainty in the observed line intensity as a primary source of error, there are possible systematic errors. For the polarization and the reflectivity of the x-ray crystal, the uncertainties amount to about 2% according to the literature. A variation in the absolute value of the reflectivity caused by the imperfection of material used here or suppressing the energy-dependent polarization degree of the resonance line results, however, only in minor change of the line-ratio value, due to the partial compensation of the weighting function at high energies. A further source of uncertainty may arise from the variation of the trap conditions and the overlap between the electron beam and the ion cloud during the sweep of the beam energy. Estimating the change of the charge balance using theoretical resonance strength shows it to be constant within 1% for the short period of the energy ramp. Since the electron-beam current is kept fixed during the ramp, the electron density varies as function of beam energy, which is accounted for in the weight function, but also might change the beam-ion overlap and, thereby, the line intensity. Our simulations of the trap inventory suggest that the overlap increases slightly when the electron-beam energy is swept to higher values introducing an error of less than 15% in accordance with measurements [36]. Adding the uncertainties with their statistical weights, we arrive at a value of 17% for the $(j+z)/w$ line ratio.

An EBIT experiment with its versatile monoenergetic electron beam has the unique possibility to differentiate radiation processes according to their excitation energy. By sampling the x rays emitted from the ions as a function of the exciting electron beam, the wavelength blend of the satellites and $z$ line can be separated. Using this method and a recently developed technique to simulate a Maxwellian plasma, line ratios of the $KLL$ satellites to the $w$ resonance were determined at the Lawrence Livermore National Laboratory (LLNL) EBIT by Savin *et al.* [36] for argon. Since the dielectronic satellites involving the $n=2$ level have not been individually resolved in that experiment, they are treated as one feature $\Sigma_{n=2}^{sat} = a+b+c+d+j+k+l+q+r$. The ratio of the sum of the $n=2$ satellites to the resonance line is shown in Fig. 5(b), together with a theoretical prediction using rate coefficients of Chen [33] and our measured values. In contrast to the method presented here for the Berlin EBIT experiment, which weights the spectroscopic line intensities with the appropriate electron-energy distribution for a certain plasma temperature, the LLNL-technique probes the trapped ion inventory by quickly ramping the energy and the current

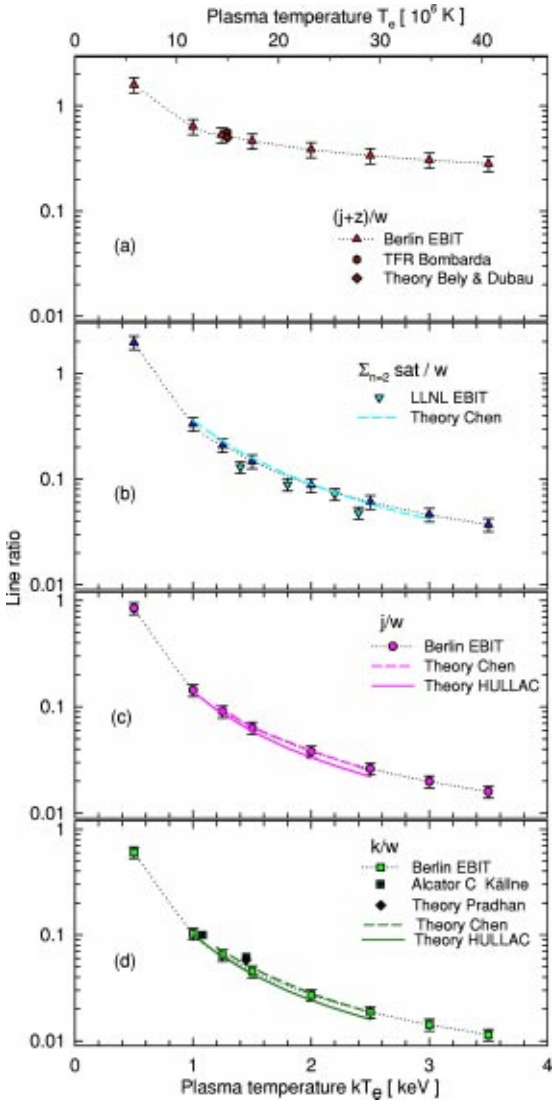


FIG. 5. Line ratios of dielectronic satellites to the $w$-resonance line of argon. Experimental values obtained from measurements at the Berlin EBIT and folded according to the plasma temperature are compared to measurements at tokamak facilities (TFR [10], Alcator $C$ [1]), the LLNL-EBIT [36], and theoretical predictions [1,33,35].

of the electron beam as a function of time to simulate a time-averaged Maxwell-Boltzmann electron-energy distribution. The two different methods to obtain information on line ratios show the same trend as a function of $T_e$ and follow the theoretical prediction.

Our combination of high-resolution spectroscopy with an EBIT experiment provides the possibility to disentangle the line blend of $j+z$ by observing spectra at different excitation energies of the electron beam and resolving the $j$ line from other satellite transitions. The line ratio of the individual $j$ satellite to the $w$-resonance line is plotted as a function of the plasma temperature in Fig. 5(c). The experimental data points follow, within the error bars, theoretical calculations using the autoionization rates of Chen [33] and HULLAC collisional excitation rate coefficients [32] [Eq. (15)], and a CR calculation [Eq. (9)] at $n_e=10^{12}$ cm$^{-3}$, with cascades from levels with $n\leqslant 6$, using only HULLAC data. For lower plasma temperatures, the measured values seem to fit best with the HULLAC predictions, while Chen's data predict larger line ratios. At the higher plasma temperatures, the trend is reversed, which might indicate a different contribution from cascades into the upper level of the $w$ line in the HULLAC calculation.

Further, we have measured and extracted the line ratio between the $k$ satellite and the $w$-resonance line as a function of the plasma temperature. The $k/w$ line ratio is plotted in Fig. 5(d) and compared to experimental values obtained at the Alcator $C$ tokamak and a calculated value using excitation rates by Pradhan [1]. In the temperature range 1–2.5 keV, theoretical calculations of the line ratio using the HULLAC package and using the DR data by Chen [33] mark the functional trend that is followed by the Berlin EBIT measurement and display slight deviations similar to those seen in the $j/w$ ratio. The $k/w$ ratio shows a much stronger temperature dependence than the $(j+z)/w$ ratio, which results in a more accurate determination of the plasma temperature from the measured $k/w$ line ratio. While an uncertainty of 17% in the $(j+z)/w$ ratio leads to a 15% error in obtaining the plasma temperature around $T_e=2$ keV, this can be improved by using the $k$ satellite to resonance line ratio. With a modest accuracy of 13% in the measured $k/w$ ratio, which is the total experimental uncertainty, the value for the plasma temperature is fixed to within 5%. This sensitivity is important for consideration in plasma diagnostic applications, where a maximum response in the measured line ratio is desirable. The wavelength separation of the $k$ line from all other spectral features in heliumlike argon allows also the extraction of the $k/w$ line ratio from tokamak spectra with modest spectroscopic effort and establishes the $k/w$ ratio as plasma-temperature diagnostic.

## V. CONCLUSION

We have measured with an EBIT the wavelength-resolved $KLL$ dielectronic recombination satellite and direct-excitation process of heliumlike argon as a function of excitation energy. From the intensity ratio of individual satellites to the resonance line folded with the energy distribution of the exciting electrons, the plasma temperature can be determined. For the comparison with tokamak experiments and theoretical predictions, a Maxwell-Boltzmann energy distribution is assumed here. However, from the data information on possible deviations from the Maxwellian can also be provided. In particular, the ratio of the $k$ satellite to the $w$-resonance line is well suited for electron-temperature diagnostics, since their distinct lines are easily resolved by spectroscopy and the line ratio is a steep function of temperature. The measured line ratios are in good agreement with results obtained at tokamak facilities and are supported by HULLAC-predicted collisional excitation rates. Modifications of the calculation by employing different atomic potentials and radiative cascade models or different collision data show only a minor influence on the line ratio, which cannot be distinguished within the experimental uncertainty. Similarly, the electron density has only a small effect on the line ratio. The experimental value for the line ratio $R$ is in agreement with theoretical predictions and the HULLAC model including the two-photon decay from the $1s2s\,^1S_0$ level to $1s^2$, which shows no density dependence.

## ACKNOWLEDGMENTS

We would like to thank Professor G. Fussmann for helpful discussions and Dr. G. Bertschinger (FZ Jülich) for pointing out the problem of this line ratio measurement. The work of one of us (K.F.) was performed under the auspices of the US Department of Energy by University of California Lawrence Livermore National Laboratory under Contract No. W-7405-Eng-48.

[1] E. Källne, J. Källne, and A.K. Pradhan, Phys. Rev. A **28**, 467 (1983).
[2] K.J. Phillips, F.P. Keenan, L.K. Harra, S.M. McCann, E. Rachlew-Källne, J.E. Rice, and M. Wilson, J. Phys. B **27**, 1939 (1994).
[3] A.H. Gabriel, Mon. Not. R. Astron. Soc. **160**, 99 (1972).
[4] A.B.C. Walker, Jr. and H.R. Rugge, Astrophys. J. **164**, 181 (1971).
[5] G.A. Doschek, U. Feldman, J.F. Seely, and D.L. McKenzie, Astrophys. J. **345**, 1079 (1989).
[6] T. Kato, T. Fujiwara, and Y. Hanaoka, Astrophys. J. **492**, 822 (1998).
[7] E. Silver, H. Schnopper, S. Bandler, N. Brickhouse, S. Murray, M. Barbera, E. Takacs, J.D. Gillaspy, J.V. Porto, I. Kink, N. Madden, D. Landis, J. Beeman, and E.E. Haller, Astrophys. J. **541**, 495 (2000).
[8] G. Bertschinger, W. Biel, the TEXTOR 94 Team, O. Herzog, J. Weinheimer, H.J. Kunze, and M. Bitter, Phys. Scr., T **83**, 132 (1999).
[9] J. Weinheimer, I. Ahmad, O. Herzog, H.-J. Kunze, G. Bertschinger, W. Biel, G. Borchert, and M. Bitter, Rev. Sci. Instrum. **72**, 2566 (2001).
[10] The TFR Group, F. Bombarda, F. Bely-Dubau, P. Faucher, M.

Cornille, J. Dubau, and M. Loulergue, Phys. Rev. A **32**, 2374 (1985).
[11] J.E. Rice, R.L. Boivin, P.T. Bonoli, J.A. Goetz, R.S. Granetz, M.J. Greenwald, I.H. Hutchinson, E.S. Marmar, G. Schilling, J.A. Snipes, S.M. Wolfe, S.J. Wukitch, C.L. Fiore, J.H. Irby, D. Mossessian, and M. Porkolab, Nucl. Fusion **41**, 277 (2001).
[12] K.B. Fournier, M. Cohen, M.J. May, and W.H. Goldstein, At. Data Nucl. Data Tables **70**, 231 (1998).
[13] E. Källne, J. Källne, E.S. Marmar, and J.E. Rice, Phys. Scr. **31**, 551 (1985).
[14] A.J. Smith, P. Beiersdorfer, V. Decaux, K. Widmann, K.J. Reed, and M.H. Chen, Phys. Rev. A **54**, 462 (1996).
[15] M.R. Tarbutt, R. Barnsley, N.J. Peacock, and J.D. Silver, J. Phys. B **34**, 3979 (2001).
[16] N.J. Peacock, R. Barnsley, M.G. O'Mullane, M.R. Tarbutt, D. Crosby, J.D. Silver, and J.A. Rainnie, Rev. Sci. Instrum. **72**, 1250 (2001).
[17] C. Biedermann, T. Fuchs, G. Fussmann, and R. Radtke, in *Trapping Highly Charged Ions: Fundamentals and Applications*, edited by J.D. Gillaspy (Nova Science, New York, 2001), p. 81.
[18] R. Radtke, C. Biedermann, T. Fuchs, G. Fussmann, and P. Beiersdorfer, Phys. Rev. E **61**, 1966 (2000).
[19] I.C. Percival and M.J. Seaton, Philos. Trans. R. Soc. London, Ser. A **251**, 113 (1958).
[20] B.L. Henke, E.M. Gullikson, and J.C. Davis, At. Data Nucl. Data Tables **54**, 181 (1993).
[21] Data available at http://sergey.bio.aps.anl.gov
[22] M.K. Inal and J. Dubau, J. Phys. B **20**, 4221 (1987).
[23] A.S. Schlyaptseva, A.M. Urnov, and A. Vinogradov, P.N. Lebedev Institute Report No. 194, 1981 (unpublished).
[24] M.F. Gu, D.W. Savin, and P. Beiersdorfer, J. Phys. B **32**, 5371 (1999).
[25] A.H. Gabriel and C. Jordan, Mon. Not. R. Astron. Soc. **145**, 241 (1969).
[26] F.P. Keenan, S.M. McCann, and A.E. Kingston, Phys. Scr. **35**, 432 (1987).
[27] S.H. Glenzer, K.B. Fournier, C. Decker, B.A. Hammel, R.W. Lee, L. Lours, B.J. MacGowan, and A.L. Osterheld, Phys. Rev. E **62**, 2728 (2000).
[28] A. Bar-Shalom and M. Klapisch, Comput. Phys. Commun. **50**, 375 (1988).
[29] M. Klapisch, Comput. Phys. Commun. **2**, 239 (1971).
[30] M. Klapisch, J. Schwob, B. Fraenkel, and J. Oreg, J. Opt. Soc. Am. **67**, 148 (1977).
[31] J. Oreg, W.H. Goldstein, M. Klapisch, and A. Bar-Shalom, Phys. Rev. A **44**, 1750 (1991).
[32] A. Bar-Shalom, M. Klapisch, and J. Oreg, Phys. Rev. A **38**, 1773 (1988).
[33] M.H. Chen, At. Data Nucl. Data Tables **34**, 301 (1986).
[34] N.C. Woolsey, B.A. Hammel, C.J. Keane, A. Asfaw, C.A. Back, J.C. Moreno, J.K. Nash, A. Calisti, C. Mosse, R. Stamm, B. Talin, L.S. Klein, and R.W. Lee, Phys. Rev. E **56**, 2314 (1997).
[35] F. Bely-Dubau, J. Dubau, P. Faucher, A.H. Gabriel, M. Loulergue, L. Steenman-Clark, S. Volente, E. Antonucci, and C.G. Rapley, Mon. Not. R. Astron. Soc. **201**, 1155 (1982).
[36] D.W. Savin, P. Beiersdorfer, S.M. Kahn, B.R. Beck, G.V. Brown, M.F. Gu, D.A. Liedahl, and J.H. Scofield, Rev. Sci. Instrum. **71**, 3362 (2000).